Polarized single top quark production at leptonic colliders from broken *R* parity interactions incorporating *CP* violation

M. Chemtob and G. Moreau
Service de Physique Théorique, CE-Saclay, F-91191 Gif-sur-Yvette Cedex, France
(Received 29 October 1999; published 9 May 2000)

The contribution from the *R* parity violating interaction $\lambda'_{ijk}L_iQ_jD^c_k$ in the associated production of a top quark (antiquark) with a charm antiquark (quark) is examined for high energy leptonic colliders. We concentrate on the reaction $l^-+l^+\to(t\bar{c})+(c\bar{t})\to(b\bar{l}\bar{\nu}\bar{c})+(\bar{b}l\nu c)$ associated with the semileptonic top quark decay. A set of characteristic dynamical distributions for the signal events is evaluated and the results contrasted against those from the standard model *W*-boson pair production background. The sensitivity to parameters (*R* parity violating coupling constants and down-squark mass) is studied at the energies of the CERN LEP-II collider and the future linear colliders. Next, we turn to a study of a *CP*-odd observable, associated with the top quark spin, which leads to an asymmetry in the energy distribution of the emitted charged leptons for the pair of *CP*-conjugate final states $b\bar{l}\bar{\nu}\bar{c}$ and $\bar{b}l\nu c$. A nonvanishing asymmetry arises from a *CP*-odd phase, embedded in the *R* parity violating coupling constants, through interference terms between the *R* parity violating amplitudes at both the tree and loop levels. The one-loop amplitude is restricted to contributions from vertex corrections to the photon and *Z*-boson exchange diagram. We predict unpolarized and polarized rate asymmetries of order $O(10^{-3})$–$O(10^{-2})$. An order of magnitude enhancement may be possible should the *R* parity violating coupling constants λ'_{ijk} exhibit a hierarchical structure in the quarks and leptons generation spaces.

PACS number(s): 11.30.Er, 11.30.Hv, 12.60.Jv, 13.10.+q

I. INTRODUCTION

The flavor nondiagonal fermion-antifermion pair production $l^-l^+\to f_J\bar{f}_{J'}$, where $J\neq J'$ are flavor labels, represents a class of reactions where the high energy colliders could contribute their own share in probing new physics incorporating flavor changing and/or *CP* violation effects. As is known, the standard model contributions here are known to be exceedingly small, whereas promising contributions are generally expected in the standard model extensions. (Consult Ref. [1] for a survey of the literature.) Of special interest is the case where a top quark (antiquark) is produced in association with a lighter (charm or up) antiquark (quark). The large top quark mass entails a top quark lifetime of $\tau_{top}=[1.56\ \mathrm{GeV}(m_t/180\ \mathrm{GeV})^3]^{-1}$, significantly shorter than the QCD hadronization time, $1/\Lambda_{QCD}$, which simplifies the task of jet reconstruction [2]. The top quark polarization effects also constitute a major attraction [3–7]. The large top quark mass entails a spin depolarization time of the top quark which is longer than its lifetime, $\tau_{depol}=[1.7\ \mathrm{MeV}(180/m_t)]^{-1}>\tau_{top}$, thus providing an easy access to top quark polarization observables. Polarization studies for the top-quark–top-antiquark pair production reaction, in both production and decay, have been actively pursued in recent years [8–10]. (An extensive literature can be consulted from these references.)

It appears worthwhile to apply similar ideas to the flavor nondiagonal fermion pair production process involving single top quark production. This reaction has motivated several theoretical studies aimed at both leptonic (l^-l^+, $e\gamma$, and $\gamma\gamma$) and hadronic ($p\bar{p}$, pp) colliders. Exploratory theoretical studies have been pursued at an implicit level, via the consideration of higher dimension contact interactions [11–13], and at an explicit level, via the consideration of mechanisms involving leptoquarks [14], an extended Higgs doublet sector [15,16], supersymmetry based on the minimal supersymmetric standard model with an approximately broken *R* parity [1,17–20], quark flavor mixing [21], standard model loops and four matter generations [22,23], or higher order standard model processes with multiparticle final states, $l^-l^+\to t\bar{c}\nu\bar{\nu}$ [24]. A survey of the current studies is provided in Ref. [12].

In this work, pursuing an effort started in our previous paper [1], we consider a test of the *R* parity violating (RPV) interactions aimed at top-charm quark associated production. Our study will focus on contributions to the process $l^-l^+\to(t\bar{c})+(\bar{t}c)$ arising at the tree level from the trilinear RPV interactions $\lambda'_{ijk}L_iQ_jD^c_k$ via a $\tilde{d}_{kR}$ squark exchange. We examine the signal associated with the (electron and muon) charged semileptonic decay channel of the top quark, $t\to bW^+\to bl^+\nu$. The final states $(bl^+\nu\bar{c})+(\bar{b}l^-\bar{\nu}c)$ ($l=e,\ \mu$) consist of an isolated energetic charged lepton, accompanied by a pair of *b* and *c* quark hadronic jets and missing energy. The standard model background may arise from the *W*-boson pair production reaction $l^+l^-\to W^+W^-$ and possibly, in the case of an imperfect *b* quark tagging, from the b-$\bar{b}$ quark pair production reaction $l^+l^-\to b\bar{b}$, followed by a semileptonic decay of one of the *b* quarks, $b\to cl^-\bar{\nu}$.

The present work consists of two main parts. In the first part, we discuss the signal associated with the top quark semileptonic decay channel. We evaluate a set of characteristic dynamical distributions for the signal and for the standard model background and obtain predictions for the effective rates based on a judicious choice of selection cuts on the final state kinematical variables. Our discussion will develop

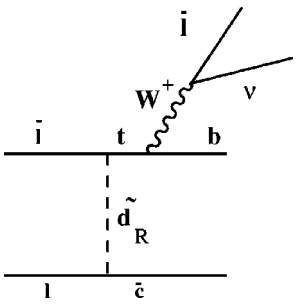

FIG. 1. Feynman diagram for the tree level amplitude of the process $l^+l^-\to\bar{c}t\to\bar{c}bl^+\nu$.

along similar lines as in a recent work of Han and Hewett [12], which was focused on the contributions initiated by the dimension, $\mathcal{D}=6$, four field couplings of the Z boson with fermion pairs, and the neutral Higgs boson. In the second part of the paper, we examine a specific CP-odd top quark polarization observable which corresponds to an asymmetry in the energy distribution of the final state charged lepton with respect to the sign of its electric charge.

The contents of the paper are organized into three sections. In Sec. II, we focus on the total and partial semileptonic decay rates for both the signal and standard model background, allowing for the case of an imperfect b quark tagging. We discuss the constraints from the indirect bounds on the RPV coupling constants, study the dependence of rates on the down-squark mass parameter, and evaluate a set of relevant dynamical distributions that are of use in devising an appropriate set of selection cuts. In Sec. III, we discuss a test of CP violation involving top quark polarization effects. The CP violating observable arises through interference terms between the tree and one-loop contributions to the amplitude and a CP-odd phase which is embodied in the RPV coupling constants. Following an approach similar to one used in earlier proposals [6,7], we describe the top quark production and decay by means of a factorization approximation and examine the induced charge asymmetry in the energy distribution of the final state charged leptons. The production amplitudes are evaluated in the helicity basis. Our main conclusions are summarized in Sec. IV.

II. TOP-CHARM QUARK ASSOCIATED PRODUCTION

A. Integrated rates

In an l^-l^+ collision, the tree level transition amplitude for single top quark production, as initiated by the RPV interactions $\lambda'_{ijk}L_iQ_jD^c_k$, proceeds via the u-channel exchange of a right-handed down-squark $\tilde{d}_{kR}$, as represented in Fig. 1. By use of a Fierz ordering identity, the transition amplitude for the flavor nondiagonal production of an up quark-antiquark pair, $l^-(k)+l^+(k')\to u_J(p)+\bar{u}_{J'}(p')$, can be written in the form of a Lorentz covariant vectorial coupling:

$$M_t^{JJ'}=-\frac{\lambda'^{\star}_{lJk}\lambda'_{lJ'k}}{2(u-m^2_{\tilde{d}_{kR}})}\bar{v}_L(k')\gamma^\mu u_L(k)\bar{u}_L(p)\gamma_\mu v_L(p'). \tag{1}$$

We shall specialize henceforth to the case of electron-positron colliders, corresponding to the choice $l=1$ for the generation index. The squared amplitude, summed over the initial and final fermion spins, reads [1]

$$\sum_{pol}|M_t^{JJ'}|^2=N_c\left|-\frac{\lambda'_{1J'k}\lambda'^{\star}_{1Jk}}{2(u-m^2_{\tilde{d}_{kR}})}\right|^2 16(k\cdot p')(k'\cdot p). \tag{2}$$

The production rate for unpolarized initial leptons, integrated over the scattering angle in the interval $0\leqslant|\cos\theta|\leqslant x_c$, is given by the analytic formula

$$\sigma=\frac{N_c|\lambda'_{1J'k}\lambda'^{\star}_{1Jk}|^2}{64\pi s^2}\left[(u_--u_+)+(2\tilde{m}^2-m_J^2-m_{J'}^2)\ln\left|\frac{u_--\tilde{m}^2}{u_+-\tilde{m}^2}\right|-(\tilde{m}^2-m_J^2)(\tilde{m}^2-m_{J'}^2)\left(\frac{1}{u_--\tilde{m}^2}-\frac{1}{u_+-\tilde{m}^2}\right)\right], \tag{3}$$

where $u_\pm=m_J^2-\sqrt{s}(E_p\pm px_c)$. For the top-charm quark associated production case, in the limit $m_J=m_t\gg m_{J'}=m_c$, one has $u_+\simeq m_t^2-s$, $u_-\simeq 0$. For fully polarized initial beams, since the RPV amplitude selects a single helicity configuration for the initial state leptons, $l_L^-l_R^+$ (left-handed l^- and right-handed l^+), the corresponding polarized rate would be still described by the same formula as above, only with an extra enhancement factor of 4. The predicted rates for $t\bar{c}$ production are controlled by quadratic products of the RPV coupling constants $\lambda'^{\star}_{13k}\lambda'_{12k}(k=1,2,3)$ and the squark mass $m_{\tilde{d}_{kR}}$, denoted for short as $\tilde{m}$. Allowing for the existence in the RPV interactions of an up-quark flavor mixing, such as would be induced by the transformation from flavor to mass basis, one may express the amplitude in terms of a single RPV coupling constant and the Cabibbo-Kobayashi-Maskawa (CKM) matrix, V, by rewriting the coupling constant dependence as $\lambda'_{12k}\lambda'^{\star}_{13k}\to\lambda'^{\star}_{1Mk}\lambda'_{1M'k}(V^\dagger)_{M'2}(V^\dagger)^{\star}_{M3}$ and selecting the maximal contribution associated with the configurations, $M=M'=2$ or 3. This yields the order of magnitude estimate $\lambda'^{\star}_{13k}\lambda'_{12k}\to|\lambda'_{12k}|^2(V^\dagger)_{22}(V^\dagger)^{\star}_{23}\approx 2|\lambda'_{12k}|^2\lambda^2$ or $2|\lambda'_{13k}|^2\lambda^2$, respectively, where $\lambda\approx\sin\theta_c\approx 0.22$, denotes the Cabibbo angle parameter.

We pause briefly to recall the current bounds on the RPV coupling constants of interest in the present study [25]. The relevant single coupling constant bounds are $\lambda'_{12k}<4.0\times10^{-2}$, $\lambda'_{13k}<0.37$ (charged current universality); $\lambda'_{1j1}<3\times10^{-2}$ (atomic physics parity violation); $\lambda'_{12k}<0.3-0.4$, $\lambda'_{13k}<0.3-0.6$ (neutral current universality); and $\lambda'_{122}<7.0\times10^{-2}$, $\lambda'_{133}<3.5\times10^{-3}$ (neutrino Majorana mass) [26]. The superpartners scalar particles masses are set at 100 GeV. Unless otherwise stated, all the dummy flavor indices for quarks and leptons are understood to run over the three generations. Using the above results for individual cou-

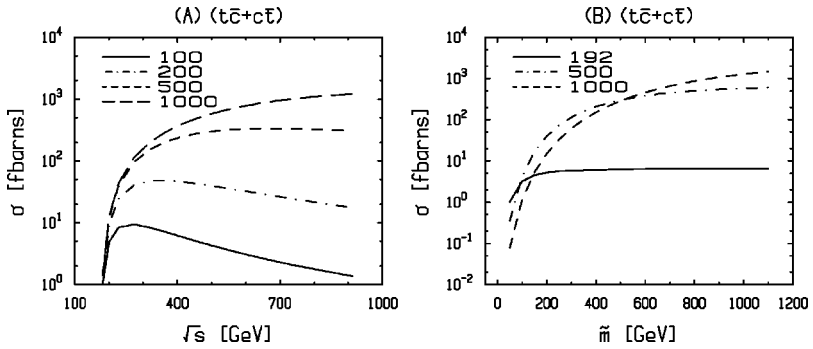

FIG. 2. The total integrated rate for the RPV-induced reaction $l^+l^-\to(t\bar{c})+(\bar{t}c)$, setting the values of the relevant coupling constants as $\lambda'_{12k}=\lambda'_{13k}=0.1(\tilde{m}/100\ \mathrm{GeV})$, is plotted in window (A) as a function of center of mass energy $s^{1/2}$ for fixed down-squark mass $\tilde{m}=[100, 200, 500, 1000]$ GeV and in window (B) as a function of $\tilde{m}$ for fixed $s^{1/2}=[192, 500, 1000]$ GeV. We integrate over an interval of the scattering angle, $0\leqslant|\cos\theta|\leqslant 0.9848$, corresponding to an opening angle with respect to the beams axis larger than 10°.

pling constants bounds, we may deduce for the following upper bounds on the relevant quadratic products [27]: $\lambda'_{13k}\lambda'_{12k}<[O(10^{-3}),\ O(10^{-2}),\ O(10^{-4})]$, $(k=1,2,3)$. The indirect quadratic product bounds $\lambda'_{ijk}\lambda'_{i'3k}<1.1\times10^{-3}$, $\lambda'_{ijk}\lambda'_{i'j3}<1.1\times10^{-3}$ $(i'=1,2)$ $(B\to X_q\nu\bar{\nu})$ are roughly comparable to these single coupling constant bounds. We also note that using the CKM flavor mixing along with a single dominant coupling constant in the current basis, as described at the end of the previous paragraph, may not be especially beneficial in avoiding the above stronger pair product bound. The bound on the corresponding coupling constant factor, $2|\lambda'_{13k}|^2\lambda^2<O(10^{-2})$, is competitive for the generation indices $k=1,3$.

Numerical results for the integrated rates have already been reported in previous works [19,1]. Setting the relevant RPV coupling constants at the reference value $\lambda'=0.1$, one predicts rates of order 1–10 fb, for $\tilde{m}=O(100)$ GeV. As the center of mass energy varies in the interval, $\sqrt{s}=192$–1000 GeV, the rates rise sharply from threshold, reaching smoothly a plateau around $\sqrt{s}\simeq400$ GeV. This contrasts with the predictions from gauge-boson-mediated higher dimension interactions [12] where the rise of the rates with incident energy is a more gradual one. The rates are also found to have a strong dependence on $\tilde{m}$, which weakens for increasing center of mass energies. One may roughly parametrize the dependence on s and $\tilde{m}$ by the approximate scaling law $\sigma\approx(\lambda'\lambda'/0.01)^2(100\ \mathrm{GeV}/\tilde{m})^{x(s)}$, where the power exponent is a fastly decreasing function of energy, taking the approximate values $x(s)\approx[3.65, 1.86, 0.94]$ at $\sqrt{s}=[0.192, 0.5, 1.0]$ TeV.

Although the predicted rates seem to be severely constrained by the above indirect bounds, one could envisage an optimistic scenario where the supersymmetry decoupling limit $\tilde{m}\to\infty$ is realized with fixed values for the products, $\lambda'_{ijk}(100\ \mathrm{GeV}/\tilde{m})\approx0.1$, consistently with the current indirect bounds. The results obtained with this prescription are displayed in Fig. 2. The integrated rates now depend on $\tilde{m}$ as $\sigma\propto(100\ \mathrm{GeV}/\tilde{m})^{-4+x(s)}$, which leads at high energies to an enhancement by up to three orders of magnitudes, compared to the case where the RPV coupling constants are taken independent of $\tilde{m}$. The initial energy of the CERN e^+e^- collider LEP-II falls right in the regime where the cross section is sharply rising with increasing initial energy. The decrease with increasing $\tilde{m}$ is stronger at LEP-II energies than at the future linear colliders energies. Note that at the largest values of the superpartner mass, $\tilde{m}\simeq1.0$ TeV, the RPV coupling constants in our prescription enter a strong coupling regime $[\lambda'=O(1)]$ and it is not clear then whether the tree level prediction makes sense.

Next, we consider the process incorporating the top quark semileptonic decay, as pictured by the Feynman diagram shown in Fig. 1. We assume that the top quark decay is dominated by the electroweak semileptonic decay channel, with branching fraction $B(t\to b+W^+)\approx1$. We also include the pair of CP-conjugate final states, $t\bar{c}$ and $c\bar{t}$ production, which multiplies the rate by a factor of 2. Note, however, that we restrict ourselves to the $u_{J'}=c$ charm quark mode only. The numerical results for rates, including a branching fraction factor of 2/9 (experimental value 21.1%) to account for the $W\to l\nu$ $(l=e,\ \mu)$ decay channels, are displayed in Table I. We also show the standard model background rate

TABLE I. Production rates for the top-charm quark production signal and the W-boson pair production background. The line entries give successively the total integrated rate for the reaction $l^+l^-\to(t\bar{c})+(c\bar{t})$ using $\lambda'=0.1$, $\tilde{m}=100$ GeV, the rate for signal events, $(b\bar{l}\bar{\nu c})+(\bar{b}l\bar{\nu}c)$, associated with the top quark semileptonic decay, the W-boson pair production background rate $l^-l^+\to W^+W^-\to(l^+\nu\bar{u}_id_j)+(l^-\bar{\nu}d_ju_i)$, and the corresponding cut signal and background rates, as obtained by applying the selection cuts quoted in the text. The results include the first two generations of charged leptons, $l=e,\ \mu$.

Energy (TeV)	0.192	0.5	1.0
Total rate σ(fb)	4.099	4.291	1.148
Signal (fb)	0.68	0.91	0.24
W^+W^- background (fb)	5076	2080	876
Cut signal (fb)	0.54	0.74	0.21
W^+W^- cut background (fb)	17.0	5.0	2.6

from the W-boson pair production, $l^-l^+ \to (W^+W^-) \to (l^+\nu\bar{u}_i d_j) + (l^-\bar{\nu}d_j u_i)$, with one W-boson decay leptonically and the other hadronically, where i, j are generation indices. The irreducible background from $W^- \to c\bar{b}$ or $W^+ \to \bar{b}c$ is strongly suppressed, due to the small branching factor, given approximately by $0.32|V_{cb}|^2 \approx 5\times 10^{-4}$. It is safer, however, to allow for the possibility where the light quark hadronic jets could be misidentified as b-quark hadronic jets. Accounting for the leptonic decay for one of the W boson and the hadronic decay for the other W boson introduces for the total rate, which includes all the subprocesses, the branching fraction factor $2(21.1\pm 0.64)\% \times (67.8\pm 1.0)\% = 0.286 \pm 0.024$. Our numerical results in Table I for the standard model background rates are in qualitative agreement with those quoted ($\sigma = [2252, 864]$ fb at $s^{1/2} = [0.5, 1.0]$ TeV) by Han and Hewett [12]. One should be aware of the existence of large loop corrections to the W^+W^- production rate, especially at high energies. The predictions including the electroweak and QCD standard model one-loop contributions read [28] $\sigma = [4624, 1647, 596]$ fb at $s^{1/2} = [0.192, 0.5, 1.0]$ TeV. We conclude therefore that our use of the tree level predictions for the W^+W^- background overestimates the true cross sections by $[9\%, 20\%, 32\%]$ at the three indicated energies.

Let us discuss briefly other possible sources of background. The next important contribution is that arising from the nonresonant W-boson virtual propagation in the amplitude with the intermediate W^+W^- bosons branching into four fermions ($l\nu q\bar{q}'$). This could be possibly estimated by subtracting the resonant contribution from the total background cross sections, weighted by suitable branching factors, as independently evaluated by numerical methods in the literature. The results for the integrated total cross sections, $l^-l^+ \to (4f) + (4f+\gamma)$ [29], including the initial state radiation and Coulomb corrections, indicate that the off-shell contributions amount to a small relative correction lower than $O(10\%)$. Alternatively, one may consider, after reconstructing the neutrino momentum from the missing energy, a procedure to impose suitable cuts on the bW invariant mass, aimed at suppressing the nonresonant production background.

One other potentially important background is that arising from the b-$\bar{b}$ quark pair production reaction $l^+l^- \to \gamma^\star/Z \to b\bar{b} \to \bar{b}(cl^-\bar{\nu}) + b(\bar{c}l^+\nu)$ [19]. The numerically derived predictions for the rates, as obtained by means of the PYTHIA generator, are $\sigma = [1.631\times 10^4,\ 2.12\times 10^3,\ 5.35\times 10^2]$ fb, at $s^{1/2} = [0.192, 0.5, 1.0]$ TeV. It would appear desirable, in view of these large predicted rates, to eliminate this background by performing a double b-quark tagging analysis on the events sample. This can be performed at a reasonably low cost, given that the detection efficiency of b-quark jets is currently set at 50%. If one performs a single b-quark tagging, the rates for the corresponding events, $l^+l^- \to \gamma^\star/Z \to b\bar{b} \to (cl^-\bar{\nu})\bar{b}$, are reduced by a branching fraction $B(b \to cl\nu) \approx 10\%$, but this is compensated by the probability of misidentifying a light quark jet as a b-quark jet, which lies at the small value of 0.4% with the current silicon vertex techniques. If no b-quark tagging is performed at all, then the above large rates may make it necessary to resort to an analysis of isolation cuts of the type to be discussed in the next subsection.

B. Distributions for the semileptonic top quark decay events

In order to separate the signal from background, we consider the same set of characteristic final state kinematical variables as proposed in the study by Han and Hewett [12]. These are the maximum and minimum energies of the two jets, E_j^{high}, E_j^{low}, the dijet invariant mass M_{jj}, the charged lepton energy E_l, and rapidity $y_l = \frac{1}{2}\log[(E_l + p_{l\|})/(E_l - p_{l\|})]$. The distributions in these six variables for the signal and background, at a center of mass energy $\sqrt{s} = 0.5$ TeV, are plotted in Fig. 3. These numerical results were obtained by means of the PYTHIA [30] event generator. One notices marked differences between signal and background. The maximum jet energy distribution is uniformly distributed for the background but sharply peaked for the signal, where the peak position is determined by the top quark mass and the incident energy as $m_t^2 = (m_c^2 - s + 2\sqrt{s}E_p)$. The minimum jet energy is uniformly distributed for both signal and background, but happily the corresponding intervals are very partially overlapping. The signal event rapidity distributions for the maximum energy jet are more central for signal than background. A similar trend holds for the lepton rapidity distributions. The dijet invariant mass is a most significant variable in discriminating against the background due to its pronounced peak at the W mass. For the signal, the dijet invariant mass is uniformly spread out. Although we do not show here the distributions for the top quark mass reconstruction, this also features a strong contrast between a strongly peaked signal and a uniform background. The lepton energy distributions for the signal and background are peaked at the opposite low and high energy ends of the physical interval, respectively. This is a familiar effect associated with the correlation between the W-boson spin polarization, which is predominantly longitudinal in the top quark decay and transverse in the direct W-boson decay, and the velocity of the emitted charged lepton. In the signal decay amplitude $t \to b\bar{l}\nu$, the fact that the left handed b quark must carry the top quark polarization forces the lepton to travel with opposite velocity to that of top quark. In the background decay amplitude $W^- \to l\bar{\nu}$, the charged lepton is emitted with a velocity pointing in the same direction as that of the W boson. Thus, the Lorentz boost effects on the emitted charged leptons act in opposite ways for the signal and background events.

While the above distinctive features between signal and background events get further pronounced with increasing center of mass energy opposite trends occur as the initial energy is lowered. The distributions at the LEP-II center of mass energy, $\sqrt{s} = 0.192$ TeV, are plotted in Fig. 4. At this energy, the monovalued distribution for the signal jet, which is now the softer lower energy jet, is still well separated from the corresponding background jet distribution. So this variable, along with the dijet invariant mass, stands up as useful a discrimation test for the signal. By contrast, the energy and

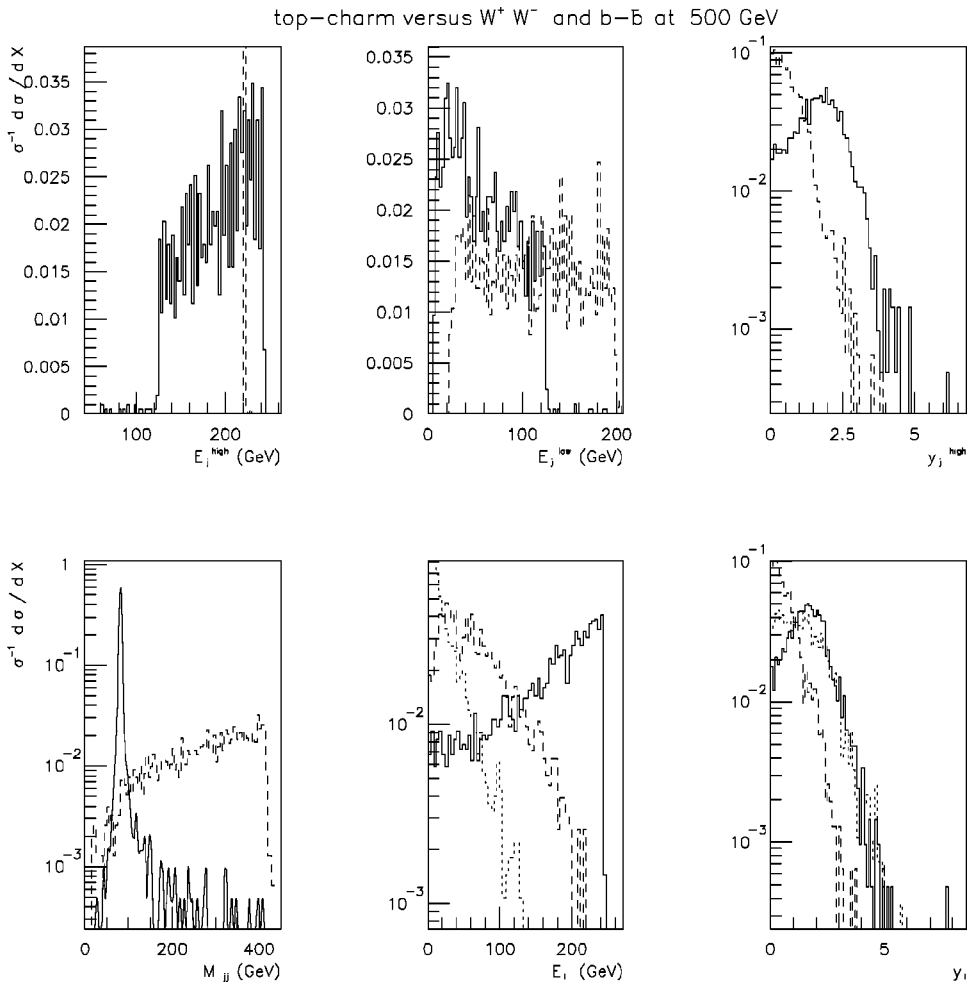

FIG. 3. Normalized dynamical distributions associated with the signal events $l^+l^- \to (t\bar{c}) + (\bar{t}c) \to (bl^+\nu\bar{c}) + (\bar{b}l^-\bar{\nu}c)$ (dashed line) at $\tilde{m} = 100$ GeV, and the background events $l^+l^- \to W^+W^- \to (l^+\nu\bar{q}q') + (l^-\bar{\nu}q\bar{q}')$ (solid line) at a center of mass energy $s^{1/2} = 500$ GeV. The kinematical variables in the histograms, from left to right and up to down, are the jet maximum energy, the jet minimum energy, the rapidity for the highest energy jet, the dijet invariant mass, the charged lepton energy, and the charged lepton rapidity. The charged lepton energy and rapidity distributions are also plotted for the b-$\bar{b}$ background production events $l^+l^- \to b\bar{b} \to l^\pm$ + hadrons (dotted line).

rapidity distributions for the maximum signal jet may not be easily distinguished from the background. Similarly, the lepton energy distributions in the signal and background are overlapping due to the small Lorentz boost effect.

The distributions obtained with the RPV interactions are rather similar to those found with the higher dimension operator mechanism [12]. This is due to the formal structure of the RPV amplitude, involving an effective u-channel vector particle exchange. In fact, the selection cuts proposed by Han and Hewett [12] appear to be quite appropriate also in the RPV case, and, for convenience, we recapitulate below the cut conditions used to characterize the selected events:

$$E_j^{low} < 20,\ E_j^{high} > 60,\ E_l > 0,\ \delta_{jj} > 10,\ \delta_t < 5\ (\sqrt{s} = 192),$$

$$E_j^{low} > 20,\ E_j^{high} > 200,\ E_l < 150,\ \delta_{jj} > 10,$$

$$\delta_t < 40\ (\sqrt{s} = 500),$$

$$E_j^{low} > 20,\ E_j^{high} > 460,\ E_l < 350,\ \delta_{jj} > 10,$$

$$\delta_t < 100\ (\sqrt{s} = 1000).$$

The above listed variables correspond to the minimum and maximum energy of the two jets, E_j^{low}, E_j^{high}, the charged lepton energy E_l, the distance between the dijet invariant mass and W-boson mass, $\delta_{jj} = |M_{jj} - m_W|$, and the distance of the reconstructed top quark mass to the true mass, $\delta_t = |m_t^{reconst} - m_t|$. The assigned numerical values are all expressed in GeV units. Besides the above cuts, we also impose the usual detection cuts on the energies and rapidities, $E_{j,l} > 10$ GeV, $|\eta_{j,l}| < 2$, aimed at removing the particles traveling too close to the beam pipe. We allow for the detection efficiency of the particle energies only in an approximate way, namely, by accounting for the approximate uncertainties $\Delta E/E = 40\%$, 10% on the jets and lepton energies, respectively, at the level of imposing the above selection cuts, rather than by the usual procedure of performing a Gaussian smearing of the particle energies.

The numerically evaluated efficiencies on the signal and background events are $\epsilon_S \simeq 0.8$, $\epsilon_B \simeq 3 \times 10^{-3}$, with a very weak dependence on the center of mass energy and, for the signal, a weak dependence on the mass parameter $\tilde{m}$, which was set at $\tilde{m} = 100$ GeV in the numerical simulations. After applying the cuts, the background rates are $\sigma_B \epsilon_B = [17.0, 5.0, 2.0]$ fb, and the signal rates $\sigma_S \epsilon_S = [0.68, 0.74, 0.21]$ fb for $\sqrt{s} = [192.0, 500.0, 1000]$ GeV. The results for the cut signal and background rates, as given in Table I, show that the background is very significantly reduced by the cuts. The situation is clearly far more favorable for future linear colliders than for LEP-II. Nevertheless,

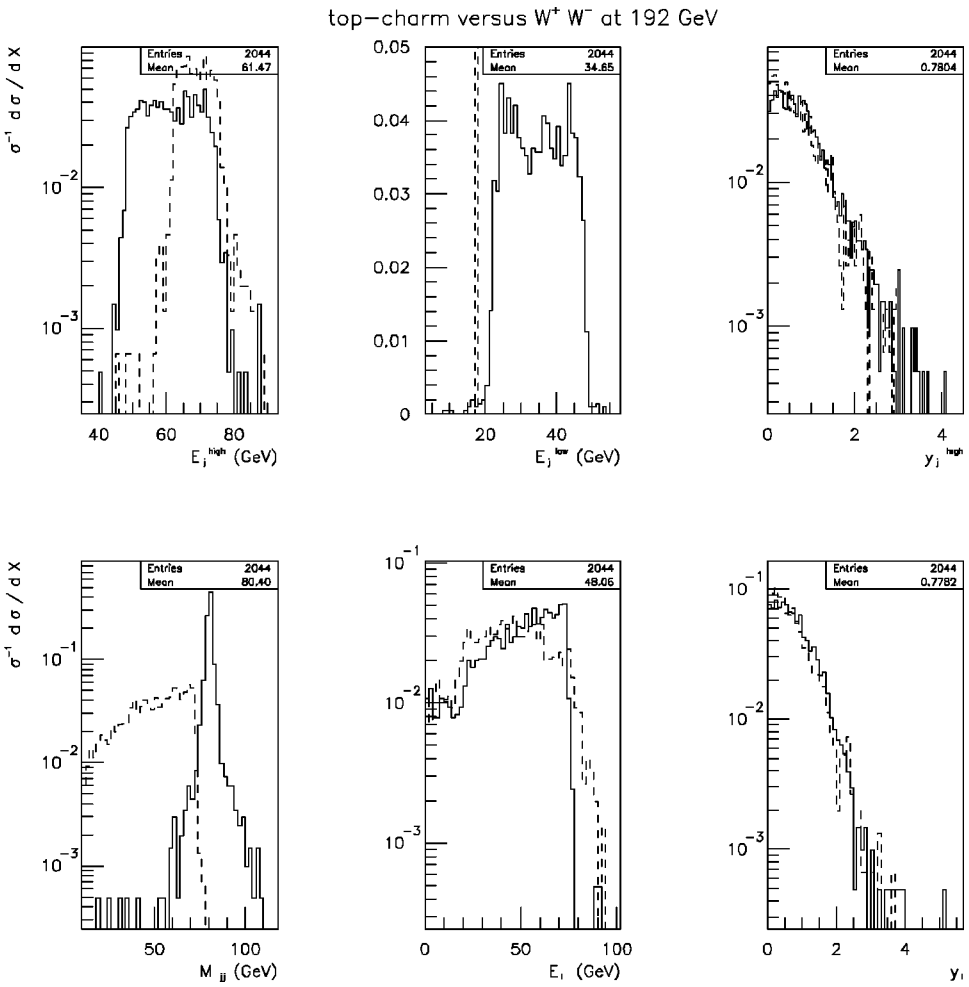

FIG. 4. Same distributions as in Fig. 3, at a center of mass energy $s^{1/2}=192$ GeV.

the number of surviving signal events is still one order of magnitude below that of the surviving background, so that the option of cutting down the background by means of a *b*-quark tagging procedure is to be preferred since the ensuing reduction would be much more drastic. An integrated luminosity of $\mathcal{L}=100$ fb^{-1} would lead to a number of signal events, $(\lambda'_{12k}\lambda'_{13k}/10^{-2})\times O(30)$.

We have also performed an indicative event generator study of the background $l^+l^-\to b\bar{b}\to l^\pm+$hadrons, restricting consideration to the emitted charged leptons only. A jet reconstruction of the partonic level distributions is a task beyond the scope of the present work. We focus on the first charged lepton emitted during the semileptonic decays of the produced B, $\bar{B}$ mesons, since this carries the largest velocity. As seen in Fig. 3, the distribution for the first emitted charged lepton energy is peaked at low energies. One expects that the most energetic lepton is that produced in the semileptonic decays of the B mesons. The rapidity distribution is less central than for the signal and nearly overlaps with that of the W^+W^- background. Therefore, imposing the additional lower bound cut on the lepton energy, say, at $E_l>20$ GeV, for $s^{1/2}=500$ GeV, should be sufficient to appreciably suppress the b-$\bar{b}$ background without much affecting the signal.

We may infer the reach with respect to the free parameters by evaluating the statistical significance ratio for a discovery, as defined by, $\hat{\sigma}=S/(\sqrt{S+B})$, $S=\sigma_S\mathcal{L}$, $B=\sigma_B\mathcal{L}$, where $\mathcal{L}$ denotes the integrated luminosity. Setting this at the value $\hat{\sigma}=3$, corresponding to a 95% confidence level, one deduces a dependence of the RPV coupling constant as a function of the superpartner mass parameters for a fixed initial energy and integrated luminosity. The sensitivity reach contour plot for the relevant parameters $\lambda'\lambda'=\lambda'_{12k}\lambda'^{\star}_{13k}$ and $\tilde{m}=m_{\tilde{d}_{kR}}$ is shown in Fig. 5. We note that the sensitivity limit on the product of coupling constants, $\lambda'\lambda'$, scales with the luminosity approximately as $1/\sqrt{\mathcal{L}}$. While the reach on the RPV coupling constants products $\lambda'_{12k}\lambda'_{13k}<O(10^{-1})$ lies well above the current indirect bounds, this covers a wide interval of the down-squark mass which extends out to 1 TeV. To compare with analogous collider physics processes, we note that while the flavor diagonal fermion pair production reactions $e^-e^+\to f_J\bar{f}_J$ may have a higher sensitivity reach, these are limited to information on the single coupling constants λ'_{1jk} [31]. The special reaction $e^-e^+\to b\bar{b}$, proceeding via a sneutrino *s*-channel resonance, may probe quadratic products such as $\lambda_{131}\lambda'_{333}$ [32] or $\lambda_{131}\lambda'_{311}$ [33] at levels of $O(10^{-3})$, but this is subject to the existence of a wide sneutrino resonance. The $t\bar{b}$ associated production

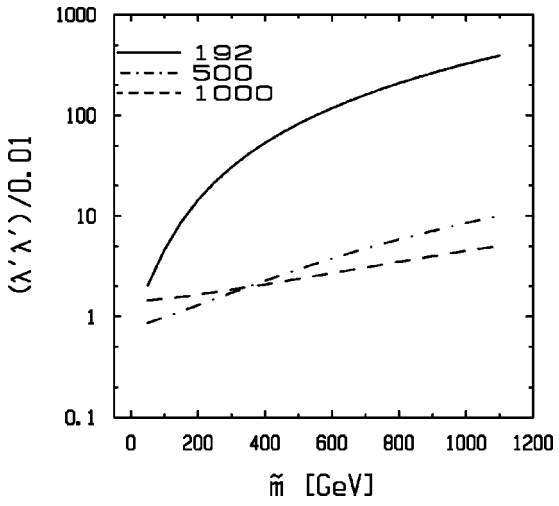

FIG. 5. Sensitivity reach plot for the RPV coupling constants product $\lambda'_{12k}\lambda'_{13k}/0.01$ as a function of the down-squark mass $\tilde{m}$ for fixed center of mass energy $s^{1/2}=[192.0, 500, 1000]$ GeV, and corresponding fixed integrated luminosity $\mathcal{L}=[2.0, 100.0, 100.0]$ fb^{-1}, using an acceptancy for the background, $\epsilon_B=3\times10^{-3}$, and an acceptance for the signal, $\epsilon_S=0.8$, assumed to be independent of $\tilde{m}$.

at the hadronic Fermilab Tevatron [17,18] and the CERN Large Hadron Collider (LHC) [18] colliders can be initiated via a charged slepton $\tilde{e}_{iL}$ s-channel exchange. The sensitivity reach on the linear combination of quadratic coupling constants products $\lambda'_{i11}\lambda'_{i33}$ is of the order of 10^{-2}–10^{-1}. This information should prove complementary to that supplied by our study aimed at the leptonic colliders. To conclude this brief comparison, we observe that the information provided by the single top quark production reaction appears to be rather unique in view of the very characteristic signature of the associated events.

III. TOP QUARK POLARIZATION OBSERVABLES AND A TEST OF *CP* VIOLATION

Should single top quark production become experimentally observable in the future, an important next step to take is in examining top quark polarization observables. In this section, we present an approximate study for the top quark semileptonic decay signal in top-charm quark associated production aiming at a test of CP violation. We exploit an idea which was developed in early studies of t-$\bar{t}$ production [5,6]. Interesting extensions are currently pursued [8–10]. The basic observation is that any CP-odd quantity depending on the top quark polarization, such as the difference of rates between the pair of CP-conjugate reactions $\sigma(l^-l^+\to t_L\bar{c})-\sigma(l^-l^+\to\bar{t}_Rc)$, can become observable by analyzing the top quark polarization through the kinematical distributions of its emitted decay (b-quark or charged-lepton) products. An especially interesting observable is the charged-lepton energy distribution for a polarized top quark. Any finite contribution to the CP-odd observables must arise through an interference term involving imaginary parts of loop and tree amplitudes factors, the loop amplitude factor bringing a CP-even final state interaction complex phase with the CP-odd relative complex phase arising from the coupling constants in the product of loop and tree amplitudes.

A. Helicity basis amplitudes

Building on our previous work [1], we shall combine the tree-level RPV-induced amplitude discussed in Sec. II with the one-loop RPV-induced amplitude associated with the photon and Z-boson exchange diagrams, restricting ourselves to the vertex corrections in the electroweak neutral current vertices, $\gamma\bar{f}_J(p)f_{J'}(p')$ and $Z\bar{f}_J(p)f_{J'}(p')$. The Z-boson vertex admits the general Lorentz covariant decomposition

$$J^Z_\mu=-\frac{g}{2\cos\theta_W}\Gamma^{JJ'}_\mu(Z),$$

$$\Gamma^{JJ'}_\mu(Z)=\gamma_\mu[A^{JJ'}_L(f)P_L+A^{JJ'}_R(f)P_R]+\frac{1}{m_J+m_{J'}}\sigma_{\mu\nu}(p+p')^\nu\times(ia^{JJ'}+\gamma_5 d^{JJ'}),\tag{4}$$

where the vectorial vertex functions $A^{JJ'}_{L,R}=A^{JJ'}_{L,R}|_{tree}+A^{JJ'}_{L,R}|_{loop}$ have a tree level contribution given by $A^{JJ'}_{L,R}|_{tree}=\delta_{JJ'}a_{L,R}(f)$, $a_{L,R}(f)=2T^{L,R}_3(f)-2Q(f)\sin^2\theta_W$, and the tensorial vertex functions $a^{JJ'}$, $d^{JJ'}$ are associated with the anomalous transition magnetic moment and the CP-odd, P-odd electric transition dipole moment, respectively. An analogous decomposition applies for the photon, $J^\gamma_\mu=-(g\sin\theta_W/2)\Gamma^{JJ'}_\mu(\gamma)$, with $a_{L,R}(f)=2Q(f)$ determined by the electric charge $Q(f)$. It is convenient to work with the $Zf_J\bar{f}_{J'}$ vertex in the alternate Lorentz covariant decomposition $\Gamma^{JJ'}_\mu(Z)=\gamma_\mu(\mathcal{A}-\mathcal{B}\gamma_5)+\frac{1}{2}(p-p')_\mu(\mathcal{C}-\mathcal{D}\gamma_5)$, where the vertex functions $\mathcal{A}$, $\mathcal{B}$, $\mathcal{C}$, $\mathcal{D}$ (omitting the up quarks generation indices J, J' for convenience) are related to the previously defined vectorial and tensorial ones, Eqs. (4), as

$$\mathcal{A}=\frac{1}{2}[A^{JJ'}_L(f)+A^{JJ'}_R(f)]+a^{JJ'},$$

$$\mathcal{B}=\frac{1}{2}[A^{JJ'}_L(f)-A^{JJ'}_R(f)]+\frac{m_J-m_{J'}}{m_J+m_{J'}}id^{JJ'},$$

$$\mathcal{C}=-\frac{2}{m_J+m_{J'}}a^{JJ'},\quad \mathcal{D}=-\frac{2}{m_J+m_{J'}}id^{JJ'}.\tag{5}$$

The one-loop Z-boson exchange amplitude may then be written in the form

$$M_l^{JJ'}(Z)=\left(\frac{g}{2\cos\theta_W}\right)^2\overline{v}(\vec{k}',\mu')\gamma_\sigma[a(e_L)P_L+a(e_R)P_R]\times u(\vec{k},\mu)\frac{1}{s-m_Z^2+im_Z\Gamma_Z}\overline{u}(\vec{p},\lambda)\times\left[\gamma^\sigma(\mathcal{A}-\mathcal{B}\gamma_5)+\frac{1}{2}(p-p')^\sigma\times(\mathcal{C}-\mathcal{D}\gamma_5)\right]v(\vec{p}',\lambda'). \quad (6)$$

Combining the above loop amplitude with the RPV tree amplitude, Eq. (1), which we rewrite as

$$M_t^{JJ'}=\mathcal{R}\overline{v}\gamma_\mu(1-\gamma_5)u\overline{u}\gamma^\mu(1-\gamma_5)v,\quad \mathcal{R}=-\frac{\lambda'^{\star}_{1Jk}\lambda'_{1J'k}}{8(u-m^2_{\tilde{d}_{kR}})}, \quad (7)$$

one obtains

$$\begin{aligned}M^{JJ'}&=M_t^{JJ'}+M_l^{JJ'}(Z)\\&=[(Ga^+\mathcal{A}+\mathcal{R})(\gamma_\mu)(\gamma^\mu)\\&\quad-(Ga^+\mathcal{B}+\mathcal{R})(\gamma_\mu)(\gamma^\mu\gamma_5)\\&\quad-(Ga^-\mathcal{A}+\mathcal{R})(\gamma_\mu\gamma_5)(\gamma^\mu)\\&\quad+(Ga^-\mathcal{B}+\mathcal{R})(\gamma_\mu\gamma_5)(\gamma^\mu\gamma_5)]+\frac{1}{2}(p\\&\quad-p')^\mu[Ga^+\mathcal{C}(\gamma_\mu)(1)-Ga^+\mathcal{D}(\gamma_\mu)(\gamma_5)\\&\quad-Ga^-\mathcal{C}(\gamma_\mu\gamma_5)(1)+Ga^-\mathcal{D}(\gamma_\mu\gamma_5)(\gamma_5)], \quad (8)\end{aligned}$$

where $a^\pm=\frac{1}{2}[a_L(e)\pm a_R(e)]$, and we have omitted writing the contractions of the Dirac spinors indices for the initial and final fermions, respectively. The photon exchange contribution can be incorporated by treating the parameters $a^\pm$ as operators acting on the vertex functions $\mathcal{A}$, $\mathcal{B}$, $\mathcal{C}$, $\mathcal{D}$ by means of the formal substitutions

$$\begin{aligned}Ga^\pm\mathcal{A}&=G_Z\frac{a_L(e)\pm a_R(e)}{2}\left(\frac{A_L^{JJ'}(f)\pm A_R^{JJ'}(f)}{2}+a^{JJ'}\right)\\&\quad+G_\gamma\begin{pmatrix}2Q(f)\\0\end{pmatrix}\left(\frac{A_L^{\gamma JJ'}(f)\pm A_R^{\gamma JJ'}(f)}{2}+a^{JJ'}\right),\\G_Z&=\left(\frac{g}{2\cos\theta_W}\right)^2\frac{1}{s-m_Z^2+im_Z\Gamma_Z},\\G_\gamma&=\left(\frac{g\sin\theta_W}{2}\right)^2\frac{1}{s}. \quad (9)\end{aligned}$$

Analogous formulas to the above ones hold for the other products $Ga^\pm\mathcal{B}$, $Ga^\pm\mathcal{C}$, $Ga^\pm\mathcal{D}$. We have labeled the vertex functions for the photon current by the suffix γ. The formulas expressing the RPV one-loop contributions to the vertex functions are provided in the Appendix, quoting the results derived in our previous work [1]. The amplitude $M^{JJ'}$ in Eq. (8) may be viewed as a 4×4 matrix in the fermions polarization space $\langle f(p,\lambda)\overline{f}_{J'}(p',\lambda')|M|l^+(k',\mu')l^-(k,\mu)\rangle$. The various products in Eq. (8) for the matrix elements with respect to the two pairs of Dirac spinors separate into eight distinct terms. The calculation of the helicity amplitudes is most conveniently performed with the help of the MATHEMATICA package. Of the 16 configurations only the 8 helicity off diagonal configurations in the initial fermions are nonvanishing. The explicit formulas for the helicity amplitudes are provided in the Appendix.

B. Charged-lepton energy distribution

The differential cross section for top quark production and decay is described in the factorization approximation. Ignoring the spin correlations, which corresponds to dropping the spin nondiagonal contributions between the production and decay stages, yields

$$\begin{aligned}d\sigma&=\frac{|p|}{128\pi s|k|}\frac{m_t}{\pi}\int d(\cos\theta)\\&\quad\times\sum_\lambda|M_{prod}(l^-l^+\to t_\lambda\overline{c})|^2\\&\quad\times\int dp^2\frac{1}{|p^2-m_t^2+im_t\Gamma_t|^2}d\Gamma_t,\\d\Gamma_t&=\frac{1}{(2\pi)^3 8m_t}\overline{\sum}_{\lambda'}|M_{dec}(t_{\lambda'}\\&\quad\to bl^+\nu)|^2dE_l^\star dE_b^\star. \quad (10)\end{aligned}$$

The production amplitude is denoted M_{prod}, the top quark decay amplitude M_{dec}, and λ, $\lambda'=\pm1$ are polarization labels, which will also be written for short as $\pm$. We shall assume a narrow resonance approximation for the top quark propagator, $|p^2-m_t^2+im_t\Gamma_t|^{-2}\to(\pi/m_t\Gamma_t)\delta(p^2-m_t^2)$. For the energies of interest, all the leptons and quarks, with the exception of the top quark , may be treated as massless. Two frames of interest are the laboratory (l^-l^+) rest frame and the top quark rest frame. The letters denoting momentun variables in the l^-l^+ center of mass (laboratory) frame are distinguished from those in the top quark rest frame by the addition of a star. Standard kinematical methods [34] can be used to transform variables between these frames. Exploiting the rotational invariance, one may conveniently choose to work in the spatial frame where the top quark momentum lies in the xOz plane ($\theta,\phi=0$) and the charged lepton points in an arbitrary direction described by the spherical angles θ_l,ϕ_l. The relations between angles may be obtained by use of the spherical triangle identities; for example, the angle between lepton and top quark reads $\cos\theta_{lt}=\cos\theta_l\cos\theta+\sin\theta_l\sin\theta\cos\phi_l$. The Lorentz boost from the top quark rest frame to the laboratory frame involves a velocity param-

eter $\vec{v}=\vec{p}/E_p$, $\beta=p/E_p$, $\gamma=(1-\beta^2)^{-1/2}=E_p/m_t$, and yields for the charged-lepton momentum four vector and polar angles relative to the top quark momentum, $E_l^\star=\gamma(E_l-\vec{v}\cdot\vec{k}_l)$, $\vec{k}_l^\star=\vec{k}_l+\gamma\vec{v}[\gamma\vec{v}\cdot\vec{k}_l/(\gamma+1)-E_l]$, $\cos\theta_{lt}^\star=(\cos\theta_{lt}-\beta)/(1-\beta\cos\theta_{lt})$.

The top quark differential semileptonic decay rate has been thoroughly studied in the literature [35]. One representation convenient for our purposes is the double differential rate with respect to the final charged-lepton energy $E_l^\star$ and the final lepton and neutrino invariant mass squared, $W^2=(k_l+k_\nu)^2$. The result for the unpolarized rate carries no dependence on the scattering angles and reads, quoting from Ref. [35],

$$\begin{aligned} d\Gamma_t &= \frac{N_l G_F^2 m_t^5}{16\pi^3} dx_l \int dy \frac{x_l(x_M-x_l)}{(1-y\xi)^2+\gamma^2}, \\ &= \frac{N_l G_F^2 m_t^5}{16\pi^3} \frac{2}{m_t} \frac{x_l(x_M-x_l)}{\gamma\xi} \\ &\quad \times \tan^{-1}\frac{\gamma\xi x_l(x_M-x_l)}{(1+\gamma^2)(1-x_l)-\xi x_l(x_M-x_l)} dE_l^\star . \end{aligned} \tag{11}$$

The kinematical variables for the emitted charged lepton and neutrino are defined as $x_l=2E_l^\star/m_t$, $y=W^2/m_t^2$ ($W=k_l+k_\nu$), with the bounds $0<x_l<x_M$, $0<y<x_l(x_M-x_l)/(1-x_l)$, and we employ the following notations: N_l for the number of light lepton flavors, $\gamma=\Gamma_W/m_W$, $\xi=m_t^2/m_W^2$, $x_M=1-\epsilon^2$, $\epsilon=m_b/m_t$, $\tan^{-1}A=\arctan|A|+\pi\theta(-A)$. Recall that the number of light lepton flavors, N_l, is set to $N_l=2$ in our analysis. A useful trick to obtain the distribution with respect to the laboratory frame lepton energy E_l is to choose the top quark momentum along the Oz axis fixed frame and introduce the top quark rest frame electron energy by means of the change of variable $(E_l,\cos\theta_l^\star)\to(E_l,E_l^\star)$, associated with the Lorentz boost between the top quark rest frame and the laboratory frame, $E_l=\gamma E_l^\star(1+\beta\cos\theta_l^\star)$. The result reads

$$\begin{aligned} \frac{d\Gamma_t}{dE_l} &= \int_{-1}^{+1} d\cos\theta_l^\star \frac{d^2\Gamma_t}{dE_l d\cos\theta_l^\star} \\ &= \frac{2}{m_t\gamma\beta}\int_{x_l^-}^{x_l^+}\frac{dx_l}{x_l}\frac{d^2\Gamma_t}{dx_l d\cos\theta_l^\star}, \end{aligned} \tag{12}$$

where the integration interval over x_l is bounded at $x_l^\pm=2E_l/[m_t\gamma(1\pm\beta)]$.

C. Top quark polarization observables

An essential use will be made of the factorization property of the double differential distribution for the top quark decay semileptonic rate with respect to the emitted lepton energy and angle relative to the top quark spin polarization vector. This distribution is described at the tree level as

$$\frac{d^2\Gamma_t}{dE_l^\star d\cos\psi_l}=\frac{d\Gamma_t}{dE_l^\star}\frac{1+\cos\psi_l}{2}$$

where $\cos\psi_l=-s(p)\cdot k_l$ is the angle between the lepton momentum and the top quark spin polarization vector $s_\mu(p)$ in the top quark rest frame. Equivalently,

$$\frac{d^2\Gamma_t}{dx_l d\cos\theta_l^\star}=\frac{d\Gamma_t}{dx_l}\frac{1+\cos\psi_l}{2}\frac{d\cos\psi_l}{d\cos\theta_l^\star}.$$

As it turns out, this representation remains valid to a good approximation when one-loop QCD corrections are included [36]. We choose to describe the top quark polarization in the spin helicity formalism, using techniques familiar from previous works [5,37]. The definition for the helicity basis Dirac spinors is provided in the Appendix. Since the polarization axis coincides then with the top quark momentum, the dependence on ψ_l can also be simply rewritten as $(1+\cos\psi_l)/2=(1+\lambda\cos\theta_l^\star)/2$, such that $\lambda=[-1,+1]$ correspond to $[L,R]$ helicity, respectively.

The helicity amplitudes associated to the pair of CP-conjugate processes are related by the action of CP as $\langle f_\lambda\bar{f}'_{\lambda'}|M|l^+_{\mu'}l^-_\mu\rangle\to\langle f'_{-\lambda'}\bar{f}_{-\lambda}|M|l^+_{-\mu}l^-_{-\mu'}\rangle$. Unlike the process $l^+l^-\to t\bar{t}$, where both the initial and final states are self-conjugate under CP, here only the initial state is self-conjugate, while the action of CP relates the different final states $t\bar{c}$ and $c\bar{t}$. Let us express the amplitudes for the pair of CP-conjugate processes as sums of tree and loop terms, $M^{JJ'}=a_0+\Sigma_\alpha b_\alpha f_\alpha(s+i\epsilon)$, $\bar{M}^{JJ'}=a_0^\star+\Sigma_\alpha b_\alpha^\star f_\alpha(s+i\epsilon)$, where the loop terms $b_\alpha f_\alpha(s+i\epsilon)$ are linear combinations with real coefficients of the vertex functions $A_L^{JJ'}$, $A_R^{JJ'}$, $a^{JJ'}$, $id^{JJ'}$, with the energy-dependent complex functions $f_\alpha(s+i\epsilon)$ representing the factors in loop amplitudes which include the absorptive parts. In terms of this notation, a CP asymmetry associated with the difference of rates for the pair of CP-conjugate processes in some given CP-conjugate configurations of the particles polarizations can be written schematically as

$$\begin{aligned} &|\langle\lambda\lambda'|M|\mu'\mu\rangle|^2-|\langle-\lambda'-\lambda|M|-\mu-\mu'\rangle|^2 \\ &\propto\sum_\alpha \mathrm{Im}(a_0 b_\alpha^\star)\mathrm{Im}[f_\alpha(s+i\epsilon)] \\ &\quad -\sum_{\alpha<\alpha'}\mathrm{Im}(b_\alpha b_{\alpha'}^\star)\mathrm{Im}[f_\alpha(s+i\epsilon)f_{\alpha'}^\star(s+i\epsilon)]. \end{aligned} \tag{13}$$

Thus, the necessary conditions for a nonvanishing polarized asymmetry to arise from the tree-loop interference term are a relative complex CP-odd phase between the tree and loop coupling constants and an absorptive part from the loop terms. The angle-integrated production rates for the CP-conjugate reactions $l^+l^-\to t\bar{c}$ and $l^+l^-\to c\bar{t}$ for the case of polarized top quarks and top antiquarks, respectively, are obtained by summing over the polarization of the c, $\bar{c}$ quarks as

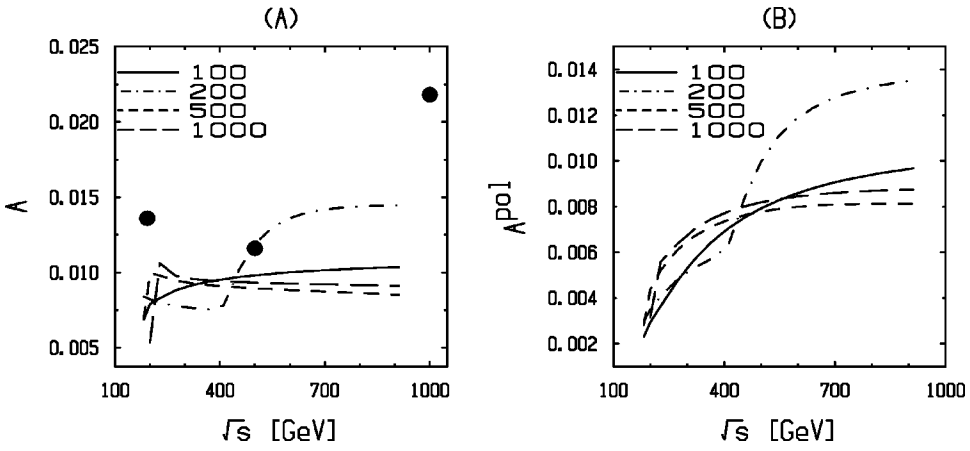

FIG. 6. The CP-odd production rate asymmetries as a function of the center of mass energy, $s^{1/2}$, for fixed values of the down squark mass $\tilde{m}=[100, 200, 500, 1000]$ GeV. The left-hand plot (A) gives the unpolarized asymmetry $\mathcal{A}=(\sigma_{av}-\bar{\sigma}_{av})/(\sigma_{av}+\bar{\sigma}_{av})$. The upper bounds for the absolute values of the statistical errors on the asymmetries, as evaluated with $\lambda'_{12k}\lambda'_{13k}=0.1$, $\tilde{m}=100$ GeV, and integrated luminosities $\mathcal{L}=100.0$ fb^{-1}, are shown as solid circles. The right-hand plot (B) gives the spin-polarization-dependent asymmetry $\mathcal{A}^{pol}=(\delta\sigma-\delta\bar{\sigma})/(\sigma_{av}+\bar{\sigma}_{av})$.

$$\sigma(t_L)=\sigma(t_L\bar{c}_R)+\sigma(t_L\bar{c}_L),\ \sigma(t_R)=\sigma(t_R\bar{c}_L)+\sigma(t_R\bar{c}_R),$$

$$\sigma(\bar{t}_L)=\sigma(\bar{t}_Lc_R)+\sigma(\bar{t}_Lc_L),\ \sigma(\bar{t}_R)=\sigma(\bar{t}_Rc_L)+\sigma(\bar{t}_Rc_R). \tag{14}$$

Forming the half differences and sums of rates, $\delta\sigma=\frac{1}{2}[\sigma(t_L)-\sigma(t_R)]$, $\delta\bar{\sigma}=\frac{1}{2}[\sigma(\bar{t}_R)-\sigma(\bar{t}_L)]$, $\sigma_{av}=\frac{1}{2}[\sigma(t_L)+\sigma(t_R)]$, $\bar{\sigma}_{av}=\frac{1}{2}[\sigma(\bar{t}_R)+\sigma(\bar{t}_L)]$, such that $\sigma(t_{L,R})=\sigma_{av}\pm\delta\sigma$, $\bar{\sigma}(t_{R,L})=\bar{\sigma}_{av}\pm\delta\bar{\sigma}$, one can define the following two CP-odd combinations:

$$\mathcal{A}=\frac{\sigma_{av}-\bar{\sigma}_{av}}{\sigma_{av}+\bar{\sigma}_{av}}=\frac{\sigma_{tc}-\sigma_{\bar{t}c}}{\sigma_{tc}+\sigma_{\bar{t}c}},\quad \mathcal{A}^{pol}=\frac{\delta\sigma-\delta\bar{\sigma}}{\sigma_{av}+\bar{\sigma}_{av}}, \tag{15}$$

which will be designated as unpolarized and polarized integrated rate asymmetries. The above definition for the unpolarized asymmetry $\mathcal{A}$ is identical to the one studied in our previous work [1]. The asymmetries depend on the RPV coupling constants through the ratio of loop to tree amplitudes as $\mathrm{Im}(\lambda'^{\star}_{iJk}\lambda'_{iJ'k}/\lambda'^{\star}_{1Jk'}\lambda'_{1J'k'})\propto\sin\psi$, where the dependence on the CP violation angle parameter ψ reflects the particular prescription adopted in this study to include the CP-odd phase. The index k' refers to the d-squark generation in the tree amplitude and the indices i,k to the fermion-sfermion generations for the internal fermion-sfermion pairs

$$\begin{pmatrix} d_k \\ \tilde{e}^{\star}_{iL}\end{pmatrix},\ \begin{pmatrix} e^c_i \\ \tilde{d}_{kR}\end{pmatrix}$$

in the loop amplitude.

It is important not to confuse the above analysis with that of the top-quark–top-antiquark pair production, $l^-l^+\to t\bar{t}$, where a CP-odd asymmetry observable for a single final state may be defined in terms of the difference of helicity configurations, $\sigma(t_L\bar{t}_L)-\sigma(t_R\bar{t}_R)$. A nonvanishing value for the corresponding difference of polarized rates can only arise via tree-loop interference terms involving the absorptive part of the top quark electric dipole moment, $\mathrm{Im}(d^{JJ})$ [6,7]. One should note here that the one-loop contribution of the RPV λ' interactions to $\mathrm{Im}(d_t^{JJ})$ vanishes. Two closely related processes, which are amenable to an analogous treatment, are $b\bar{b}$-quark pair [38] and $\tau^+\tau^-$-lepton pair production. Double spin correlation observables for the latter reaction $l^-l^+\to\tau^-\tau^+$ have been examined in a recent work [39]. We note that the RPV λ interactions can give a nonvanishing contribution to $\mathrm{Im}(d_\tau^{JJ})$.

The results for the rate asymmetries are displayed in Fig. 6. The numerical results for the unpolarized case [window (A) in Fig. 6] update the results presented in Ref. [1] since the present calculation includes the contributions from the Lorentz covariant tensorial ($\sigma_{\mu\nu}$) coupling which were ignored in our previous work [1]. The asymmetry for the polarized case [window (B) in Fig. 6] involves the difference of the spin helicity asymmetry in the total production cross sections for the CP mirror conjugate top quark and top antiquark mirror reactions. While this CP-odd polarized asymmetry is not directly observable, it enters as an important intermediate quantity in evaluating the measurable kinematic distributions of the top quark decay products dependent on the top quark spin. We have assumed all the relevant RPV coupling constants to be equal and set the CP-odd phase at $\sin\psi=1$. The rapid change in slope for the $\tilde{m}=200$ GeV case is due to the threshold effect from the imaginary part in the superpartner one-loop contributions, which are set at $\sqrt{s}=400$ GeV. Aside from this large discontinuous contribution, one sees that both asymmetries comprise another contribution which is nearly independent of $\tilde{m}$ and increases smoothly with the initial energy. Both asymmetries $\mathcal{A}$ and $\mathcal{A}^{pol}$ take values of the order of a few 10^{-3}, reaching $O(10^{-2})$ at the highest incident energies.

The statistical uncertainties in the asymmetry may be evaluated in terms of the signal cross sections and the integrated luminosity by considering the approximate definition $\delta\mathcal{A}=1/[\mathcal{L}(\sigma_{tc}+\sigma_{\bar{t}c})]^{1/2}$. Using the same input value for the luminosity, $\mathcal{L}=100.0$ fb^{-1} at the three c.m. energies, $\sqrt{s}=[0.192, 0.5, 1.0]$ TeV, along with the cut signal rates in Table I, we obtain statistical errors on the asymmetries of order $O(10^{-1})$. These values lie nearly two order of magnitudes above the value obtained for the signal. At this point, it is important to observe that in getting the above estimates for the rates we have been using somewhat conservative assignments for the RPV coupling constants. As already noted, the single top quark production cross sections could possibly be two order of magnitudes larger if we were to use coupling constants values of order $\lambda'_{12k}\lambda'_{13k}\simeq 10^{-1}$. Such values are compatible with the indirect bounds only for the extreme down-squark mass $\tilde{m}=O(1\ \text{TeV})$ range. In the hypothetical case where the production rates would be enhanced by two order of magnitudes, the statistical errors in the asymmetries would correspondingly get reduced by a factor of $O(10^{-1})$, thereby reaching the same order of magnitude as the signal asymmetries. Nevertheless, as plotted in window (*A*) of Fig. 6, the corresponding errors would still be somewhat larger than the signals. We should note here that the contribution to the one-loop amplitude from internal sfermion and fermion lines belonging to the third generation is controlled by the coupling constant quadratic product $\lambda'_{323}\lambda'_{333}$, which is subject to weak constraints. Should the RPV coupling constants exhibit a hierarchical structure with respect to quark and lepton generations, one cannot exclude the possibility of a factor of 10 enhancement from the ratio $\text{Im}(\lambda'^{\star}_{323}\lambda'_{333}/\lambda'^{\star}_{123}\lambda'_{133})$. Such an order of magnitude gain in this ratio would raise the asymmetries up to $O(10^{-1})$, bringing them well above the experimental uncertainties. Last, we observe that a more complete formula for the uncertainties in the asymmetries reads $(\delta\mathcal{A})^2=2(\delta\sigma_{\bar{t}c})^2[1-C+(1+C)\mathcal{A}^2]/(\sigma_{\bar{t}c}+\sigma_{t\bar{c}})^2$, where we used equal standard deviations for the *CP*-conjugate reactions rates $\delta\sigma_{\bar{t}c}=\delta\sigma_{t\bar{c}}$ and denoted the correlated error in these two rates as $C=\langle\delta\sigma_{\bar{t}c}\delta\sigma_{t\bar{c}}\rangle/\delta\sigma^2_{\bar{t}c}$. Clearly, an improvement in the statistical treatment of the $\bar{t}c+t\bar{c}$ events sample, allowing for a positive nonvanishing value of the error correlation associated with the identification of isolated single negatively and positively charged-lepton events, should greatly help in reducing the experimental uncertainties caused by the small event rates.

The energy distribution for the negatively and positively charged leptons in the pair of CP-conjugate reactions may be defined as

$$\langle\sigma^+\rangle\equiv\left\langle\frac{d\sigma^+}{dE_l}\right\rangle=\langle\sigma(t_L)f_L+\sigma(t_R)f_R\rangle,$$

$$\langle\sigma^-\rangle\equiv\left\langle\frac{d\sigma^-}{dE_l}\right\rangle=\langle\sigma(\bar{t}_R)f_L+\sigma(\bar{t}_L)f_R\rangle, \tag{16}$$

where the correlations between the top quark spin lepton momentum are described by the factors $f_{L,R}=\frac{1}{2}(1\mp\cos\theta^{\star}_l)$ and the brackets stand for the angular integration. The occurrence of angular correlation factors of opposite signs in the $\bar{t}$ production case accounts for the kinematical fact that the top antiquark is oriented in space with a momentum $-\vec{p}$. A *CP*-odd charge asymmetry observable with respect to the charged lepton energy distribution may be defined by considering the following normalized difference of distributions:

$$\Delta\mathcal{A}^{pol}=\frac{\langle\sigma^+\rangle-\langle\sigma^-\rangle}{\langle\sigma^+\rangle+\langle\sigma^-\rangle}=\frac{(\sigma_{av}-\bar{\sigma}_{av})+\langle(\delta\sigma-\delta\bar{\sigma})(f_L-f_R)\rangle}{(\sigma_{av}+\bar{\sigma}_{av})+\langle(\delta\sigma+\delta\bar{\sigma})(f_L-f_R)\rangle}. \tag{17}$$

The numerical results for the charged lepton energy distributions and for the above-defined charge asymmetry in the lepton energy distributions are displayed in Fig. 7. [Note that the transverse energy distribution, in the plane orthogonal with respect to the top quark momentum, may be simply obtained as $d\Gamma/dE_{lT}=(d\Gamma/dE_l)(1/\sin\theta^{\star}_{lt})$. The distribution in the plane orthogonal to the collision axis is less trivial to evaluate since this requires an additional integration over the lepton azimuthal angle.] The energy distributions for the unpolarized cross section essentially reproduce the results found in our above-quoted event generator predictions, Fig. 3. The energy distributions for the polarized asymmetry lie at values of order of magnitude, $O(10^{-3})$, always retaining the same positive sign as the lepton energy varies. For a fixed energy of the emitted lepton, the asymmetry increases with the initial energy, reaching values of order $O(10^{-2})$. In window (*B*) of Fig. 7 we have plotted the experimental uncertainties using the same inputs for the luminosities and the rates as in the discussion of the unpolarized asymmetries given above. To ease the comparison with experiment, we divide the charged-lepton energy interval into three bins of width 100 GeV, each centered at the three lepton energies $E_l=(50, 150, 250)$ GeV. The statistical errors in the asymmetries in the energy distributions lie at the same level as those associated with the total asymmetries, so that similar conclusions should apply. Setting ourselves within the same optimistic scenario by using $\lambda'_{12k}\lambda'_{13k}=10^{-1}$ and $\mathcal{L}=100$ fb^{-1}, we obtain expected errors of order $O(10^{-2})$. These values are insufficient for a comfortable identification of a signal asymmetry. However, we reiterate, as in the above discussion, that an enhancement of the signal asymmetries to an observable level of $O(10^{-1})$, due to a hierarchical structure in the generation dependence of the λ'_{ijk}, is a real possibility.

IV. CONCLUSIONS

We have demonstrated that single top quark production through the RPV interactions could be observed at future linear colliders or else be used to set bounds on the RPV coupling constants $\lambda'_{12k}\lambda'_{13k}<O(10^{-2})$ over a wide interval for the down-squark mass $m_{\tilde{d}_{kR}}<1.0$ TeV. The *b*-quark tagging would help greatly to overcome the background. Even

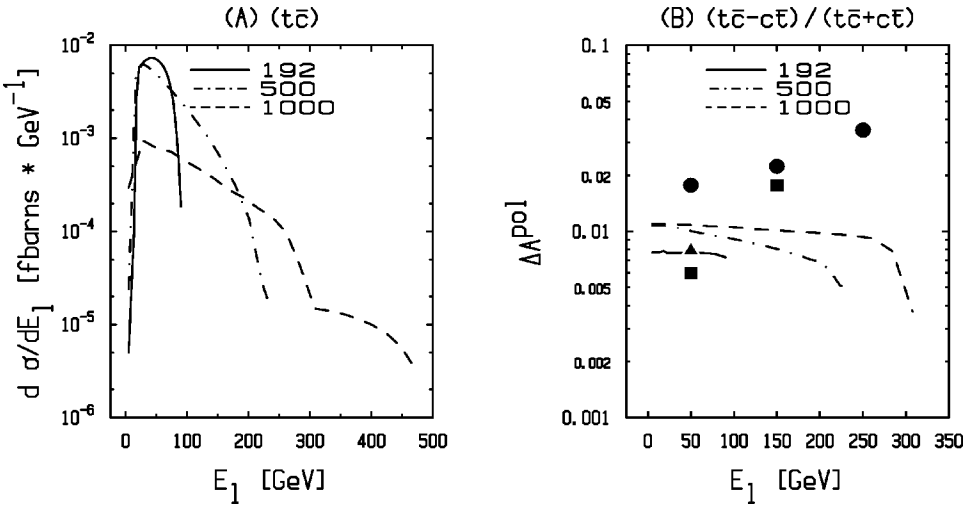

FIG. 7. Energy distribution for the charged lepton as a function of the laboratory frame lepton energy, for a set of center of mass energy $s^{1/2}=[192, 500, 1000]$ GeV. The parameters are set at $\lambda'=0.1$, $\tilde{m}=100$ GeV. The left-hand plot (*A*) gives the differential lepton energy distribution $d\sigma/dE_l$. The right-hand plot (*B*) gives the asymmetry in the energy distribution for leptons of opposite charges in the *CP*-conjugate final state channels $(t\bar{c})$ and $(c\bar{t})$: $\Delta\mathcal{A}^{pol}=[d\sigma^+/dE_l-d\sigma^-/dE_l]/[d\sigma^+/dE_l+d\sigma^-/dE_l]$. The upper bounds for the absolute values of the statistical errors on the asymmetries, as evaluated with $\lambda'_{12k}\lambda'_{13k}=0.1$ and with integrated luminosities $\mathcal{L}=100.0$ fb^{-1}, are shown for three energy bins of width 100 GeV, each centered at the charged lepton energies $E_l=(50, 150, 250)$ GeV. The results for three values of the center of mass energy $s^{1/2}=[192, 500, 1000]$ GeV are displayed by solid triangles, squares, and circles.

with an imperfect *b*-quark tagging, it is still possible to drastically reduce the background, from WW and $b\bar{b}$, without much harming the signal. The analysis of top quark polarization observables via the semileptonic decay channel of the top quark allows us to test for the presence of a *CP* violating complex phase, embedded in quadratic products of the RPV coupling constants. We have focused on the asymmetry in the energy distributions of the charged leptons in the *CP*-conjugate pair of final states $bl^+\nu\bar{c}$ and $\bar{b}l^-\bar{\nu}c$, obtaining asymmetries of order 10^{-3}–10^{-2} for the incident energies expected at future leptonic colliders. These values lie somewhat below the anticipated limits of observability. However, it may be possible to obtain enhanced values of order 10^{-1}, should the RPV coupling constants λ'_{ijk} exhibit large hierarchies with respect to quark or lepton generation. Future promising extensions might include analogous reactions accessible with lepton-photon or photon-photon colliding beams, $l\gamma\to t\bar{c}$, $\gamma\gamma\to t\bar{c}$, where the expected production rates are substantially larger than those for l^-l^+ colliders.

This work was supported by the Laboratoire de la Direction des Sciences de la Matière du Commissariat à l'Energie Atomique.

APPENDIX

Helicity Amplitudes

The helicity spin basis Dirac spinors for a fermion or an antifermion, of mass m, four-momentum $k_\mu=(E_k=(k^2+m^2)^{1/2},\vec{k})$, and polar coordinates $\vec{k}=(\theta,\phi)$, can be written in the form of direct products of the Dirac spinor two-component space with the two-component space of Pauli helicity basis spinors, $\phi_\lambda(\vec{k})$, satisfying $\vec{\sigma}\cdot\hat{k}\phi_\lambda(\vec{k})=\lambda\phi_\lambda(\vec{k})$. In the Dirac representation for the Dirac matrices,

$$\gamma_0=\beta,\ \vec{\gamma}=\beta\vec{\alpha},\ \gamma_5=\begin{pmatrix}0 & 1\\ -1 & 0\end{pmatrix},$$

the spinors read

$$u(\vec{k},\lambda)=\sqrt{\epsilon_k}\begin{pmatrix}1\\ \tilde{k}\lambda\end{pmatrix}\phi_\lambda(\vec{k}),\quad v(\vec{k},\lambda)=\sqrt{\epsilon_k}\begin{pmatrix}-\tilde{k}\lambda\\ 1\end{pmatrix}\phi_{-\lambda}(\vec{k}),$$

$$\phi_{-1}(\vec{k})=\begin{pmatrix}-\sin(\theta/2)e^{-i\phi}\\ \cos(\theta/2)\end{pmatrix},\quad \phi_{+1}(\vec{k})=\begin{pmatrix}\cos(\theta/2)\\ \sin(\theta/2)e^{+i\phi}\end{pmatrix},\tag{A1}$$

where $\epsilon_k=E_k+m$, $\tilde{k}=|\vec{k}|/(E_k+m)$, and χ_λ $(\lambda=\pm1)$, are the Pauli spinors in the basis with a fixed quantization axis identified with the spatial three-axis Oz. The helicity basis spin eigenstates with a space-parity reversed three-momentum are defined as $\phi_\lambda(-\vec{k})=e^{-i(\phi+\pi)(\lambda'-\lambda)/2}(e^{-i[(\pi-\theta)/2]\sigma_y})_{\lambda'\lambda}\chi_{\lambda'}=\phi_\lambda(\vec{k})|_{[\theta\to\pi-\theta,\ \phi\to\phi+\pi]}$.

The eight nonvanishing helicity amplitudes for the process $l^+(k',\mu')+l^-(k,\mu)\to u_J(p,\lambda)+\bar{u}_{J'}(p',\lambda')$ are listed in the formulas below:

$$\begin{aligned}M_1&=M(+--+)\\ &=4\mathcal{F}[-(1+\tilde{p}\tilde{p}')(X_1+X_2)\\ &\quad+(\tilde{p}+\tilde{p}')(X_3+X_4)]\sin^2(\theta/2),\end{aligned}$$

$$
\begin{aligned}
M_2 &= M(+-++) \\
&= 2\mathcal{F}[(-1+\tilde{p}\tilde{p}')(X_1+X_2)+(\tilde{p}-\tilde{p}')X_3 \\
&\quad +(\tilde{p}-\tilde{p}')X_4+2p(\tilde{p}+\tilde{p}')(X_5+X_6) \\
&\quad +2p(1+\tilde{p}\tilde{p}')(X_7+X_8)]\sin(\theta), \\
M_3 &= M(-++-) \\
&= -4\mathcal{F}[-(1+\tilde{p}\tilde{p}')(-X_1+X_2) \\
&\quad -(\tilde{p}+\tilde{p}')(X_3-X_4)]\cos^2(\theta/2), \\
M_4 &= M(-+++) \\
&= 2\mathcal{F}[(-1+\tilde{p}\tilde{p}')(-X_1+X_2) \\
&\quad +(-\tilde{p}+\tilde{p}')(X_3-X_4) \\
&\quad -2p(\tilde{p}+\tilde{p}')(X_5-X_6) \\
&\quad -2p(1+\tilde{p}\tilde{p}')(X_7-X_8)]\sin(\theta), \\
M_5 &= M(+---) \\
&= 2\mathcal{F}[(-1+\tilde{p}\tilde{p}')(X_1+X_2)+(-\tilde{p}+\tilde{p}')X_3 \\
&\quad +(-\tilde{p}+\tilde{p}')X_4+2p(\tilde{p}+\tilde{p}')(X_5+X_6) \\
&\quad -2p(1+\tilde{p}\tilde{p}')(X_7-X_8)]\sin(\theta), \\
M_6 &= M(+--+) \\
&= -4\mathcal{F}[(1+\tilde{p}\tilde{p}')(X_1+X_2) \\
&\quad +(\tilde{p}+\tilde{p}')(X_3+X_4)]\cos^2(\theta/2), \\
M_7 &= M(-+--) \\
&= 2\mathcal{F}[(-1+\tilde{p}\tilde{p}')(-X_1+X_2) \\
&\quad +(\tilde{p}-\tilde{p}')(X_3-X_4)-2p(\tilde{p}+\tilde{p}') \\
&\quad \times(X_5-X_6)+2p(1+\tilde{p}\tilde{p}')(X_7-X_8)]\sin(\theta), \\
M_8 &= M(-+-+) \\
&= 4\mathcal{F}[-(1+\tilde{p}\tilde{p}')(X_1-X_2) \\
&\quad -(\tilde{p}+\tilde{p}')(X_3-X_4)]\sin^2(\theta/2). \qquad \text{(A2)}
\end{aligned}
$$

The arguments refer to the fermions helicity in the following order: $M_i(h_{e^+},h_{e^-},h_f,h_{\bar{f}})$. The remaining helicity amplitudes, omitted from the above list, are understood to vanish identically. We denote by θ the top quark scattering angle $\cos\theta=\vec{k}\cdot\vec{p}$ by $[E_p,E_p']=(s\pm m_J^2\mp m_{J'}^2)/2\sqrt{s}$, the top and charm quark energies, and use the following abbreviated notation: $\tilde{p}=p/(E_p+m_J)$, $\tilde{p}'=p/(E_p'+m_{J'})$, $\mathcal{F}=\frac{1}{2}[s(E_p+m_J)(E_p'+m_{J'})]^{1/2}$, along with the useful compact notation,

$$
\begin{aligned}
X_1 &= Ga^+\mathcal{A}+\mathcal{R}, \quad X_2 = Ga^-\mathcal{A}+\mathcal{R}, \qquad \text{(A3)} \\
X_3 &= Ga^+\mathcal{B}+\mathcal{R}, \quad X_4 = Ga^-\mathcal{B}+\mathcal{R}, \\
X_5 &= \frac{1}{2}Ga^+\mathcal{C}, \quad X_6 = \frac{1}{2}Ga^-\mathcal{C}, \\
X_7 &= \frac{1}{2}Ga^+\mathcal{D}, \quad X_8 = \frac{1}{2}Ga^-\mathcal{D},
\end{aligned}
$$

where $Ga^{\pm}\mathcal{A},\ldots$ are defined in Eq. (9), $\mathcal{R}$ in Eq. (7), and $\mathcal{A},\ldots,\mathcal{D}$, in Eq. (5).

One-loop RPV vector boson vertex functions

The one-loop vertex functions, as derived in [1], are given by the formulas

$$
\begin{aligned}
A_L^{JJ'} &= \frac{\lambda'_{iJ'k}\lambda'^{\star}_{iJk}}{(4\pi)^2}\{a_L(u)B_1^{(2)}+a(f_L)m_f^2C_0+a(\tilde{f}') \\
&\quad \times[2\tilde{C}_{24}+2m_J^2(\tilde{C}_{12}-\tilde{C}_{21}+\tilde{C}_{23}-\tilde{C}_{11})] \\
&\quad +a(f_R)[B_0^{(1)}-2C_{24}-m_{\tilde{f}'}{}^2C_0+m_J^2(C_0+3C_{11} \\
&\quad -2C_{12}+2C_{21}-2C_{23})-m_{J'}^2C_{12}]\}, \\
A_R^{JJ'} &= \frac{\lambda'_{iJ'k}\lambda'^{\star}_{iJk}}{(4\pi)^2}m_Jm_{J'}[2a(\tilde{f}')(-\tilde{C}_{23}+\tilde{C}_{22}) \\
&\quad +a(f_R)(-C_{11}+C_{12}-2C_{23}+2C_{22})], \\
\begin{pmatrix} a^{JJ'} \\ -id^{JJ'} \end{pmatrix} &= \frac{\lambda'_{iJ'k}\lambda'^{\star}_{iJk}}{(4\pi)^2}\frac{m_J+m_{J'}}{4}\{\pm m_J[a(f_R)(C_{11}-C_{12} \\
&\quad +C_{21}-C_{23})-a(\tilde{f}')(\tilde{C}_{11}+\tilde{C}_{21}-\tilde{C}_{12}-\tilde{C}_{23})] \\
&\quad +m_{J'}[a(f_R)(C_{22}-C_{23})+a(\tilde{f}')(\tilde{C}_{23}-\tilde{C}_{22})]\}. \qquad \text{(A4)}
\end{aligned}
$$

The relevant configurations for the internal fermion and sfermion propagating in the loop are

$$
\begin{pmatrix} f \\ \tilde{f}' \end{pmatrix} = \begin{pmatrix} d_k \\ \tilde{e}^{\star}_{iL} \end{pmatrix}, \begin{pmatrix} e_i^c \\ \tilde{d}_{kR} \end{pmatrix}.
$$

The notation for the Passarino-Veltman two-point and three-point integrals, as specified in our work [1], is defined according to the following conventions: $B_A^{(1)}=B_A(-p-p',m_f,m_f)$, $B_A^{(2)}=B_A(-p,m_f,m_{\tilde{f}'})$ $(A=0,1)$, and $C_A=C_A(-p,-p',m_f,m_{\tilde{f}'},m_f)$, $\tilde{C}_A=C_A(-p,-p',m_{\tilde{f}'},m_f,m_{\tilde{f}'})$ $(A=0,11,12,21,22,23)$. The integral functions with a tilde are associated with the one-loop diagram for the sfermion current.

[1] M. Chemtob and G. Moreau, Phys. Rev. D **59**, 116012 (1999).
[2] C. Quigg, FERMILAB-CONF-98-059-T, hep-ph/9802320; S. Willenbrock, hep-ph/9709355; M. Beneke *et al.*, hep-ph/0003033.
[3] J. Donoghue and G. Valencia, Phys. Rev. Lett. **58**, 451 (1987); **60**, 243(E) (1988); C. A. Nelson, Phys. Rev. D **41**, 2805 (1990).
[4] D. Atwood and A. Soni, Phys. Rev. D **45**, 2405 (1992); W. Bernreuther, T. Schröder, and T. N. Pham, Phys. Lett. B **279**, 389 (1992); W. Bernreuther, O. Nachtmann, P. Overmann, and T. Schröder, Nucl. Phys. **B388**, 53 (1992); B. Grzadkowski and J. Gunion, Phys. Lett. B **287**, 237 (1992).
[5] G. L. Kane, G. A. Ladinsky, and C. P. Yuan, Phys. Rev. D **45**, 124 (1992).
[6] C. R. Schmidt and M. E. Peskin, Phys. Rev. Lett. **69**, 410 (1992); C. R. Schmidt, Phys. Lett. B **293**, 111 (1992).
[7] D. Chang and W.-Y. Keung, Phys. Lett. B **305**, 261 (1993); D. Chang, W.-Y. Keung, and I. Phillips, Nucl. Phys. **B408**, 286 (1993); **B429**, 255 (1994).
[8] W. Bernreuther and A. Brandenburg, Phys. Rev. D **49**, 4481 (1994); T. Arens and L. M. Seghal, *ibid.* **50**, 4372 (1994); P. Poulose and S. Rindani, Phys. Lett. B **349**, 379 (1995); B. Grzadkowski and Z. Hioki, Nucl. Phys. **B484**, 17 (1997); H.-Y. Zhou, Phys. Rev. D **58**, 114002 (1998).
[9] A. Bartl, E. Christova, T. Gajdosik, and W. Majerotto, Phys. Rev. D **58**, 074007 (1998); **59**, 077503 (1999).
[10] W. Hollik, J. I. Illana, S. Rigolin, C. Schappacher, and D. Stöckinger, Nucl. Phys. **B551**, 3 (1999); **B557**, 407 (1999).
[11] K.-I. Hikasa, Phys. Lett. **149B**, 221 (1984).
[12] T. Han and J. L. Hewett, Phys. Rev. D **60**, 074015 (1999).
[13] K. J. Abraham, K. Whisnant, and B.-L. Young, Phys. Lett. B **419**, 381 (1998).
[14] V. Barger and H. Hagiwara, Phys. Rev. D **37**, 3320 (1988).
[15] D. Atwood, L. Reina, and A. Soni, Phys. Rev. D **53**, 1199 (1996); **55**, 3157 (1997); Phys. Rev. Lett. **75**, 3800 (1995).
[16] D. Atwood, S. Bar-Shalom, G. Eilam, and A. Soni, Phys. Rev. D **54**, 5412 (1996).
[17] A. Datta, J. M. Yang, B.-L. Young, and X. Zhang, Phys. Rev. D **56**, 3107 (1997).
[18] R. J. Oakes, K. Whisnant, J. M. Yang, B.-L. Young, and X. Zhang, Phys. Rev. D **57**, 534 (1998).
[19] V. Mahanta and A. Ghosal, Phys. Rev. D **57**, 1735 (1998).
[20] Z.-H. Yu, H. Pietschmann, W.-G. Ma, L. Han, and J. Yi, hep-ph/9903471; hep-ph/9910323.
[21] Y. Koide, hep-ph/9701261.
[22] C. H. Chang, X.-Q. Li, J.-X. Wang, and M.-Z. Yang, Phys. Lett. B **313**, 389 (1993).
[23] C. S. Huang, X.-H. Wu, and S. H. Zhu, Phys. Lett. B **452**, 143 (1999).
[24] S. Bar-Shalom, G. Eilam, A. Soni, and J. Wudka, Phys. Rev. Lett. **79**, 1217 (1997); Phys. Rev. D **57**, 2957 (1998); W.-S. Hou, G.-L. Lin, and C.-Y. Ma, *ibid.* **56**, 7434 (1997); D. Atwood and M. Sher, Phys. Lett. B **411**, 306 (1997).
[25] G. Bhattacharyya, *Susy '96*, Nucl. Phys. B (Proc. Suppl.) **52**, 83 (1997).
[26] R. M. Godbole, R. P. Roy, and X. Tata, Nucl. Phys. **B401**, 67 (1993).
[27] Y. Grossman, Z. Ligeti, and E. Nardi, Nucl. Phys. **B465**, 369 (1996).
[28] W. Beenakker and A. Denner, Int. J. Mod. Phys. A **9**, 4837 (1994).
[29] D. Bardin, M. Bilenky, A. Olachevsky, and T. Riemann, Phys. Lett. B **308**, 403 (1993).
[30] T. Sjöstrand, Comput. Phys. Commun. **82**, 74 (1994).
[31] D. Choudhury, Phys. Lett. B **376**, 201 (1996).
[32] J. Erler, J. Feng, and N. Polonsky, Phys. Rev. Lett. **78**, 3012 (1997).
[33] J. Kalinowski, R. Rückl, H. Spiesberger, and P. M. Zerwas, Phys. Lett. B **414**, 297 (1997).
[34] E. Byckling and K. Kajantje, *Particle Kinematics*, (Wiley, London, 1973).
[35] M. Jezabek and J. H. Kühn, Nucl. Phys. **B320**, 20 (1989).
[36] A. Czarnecki, M. Jezabek, and J. H. Kühn, Nucl. Phys. **B351**, 70 (1991); M. Jezabek and J. H. Kühn, Phys. Lett. B **329**, 317 (1994).
[37] G. R. Farrar and F. Neri, Phys. Lett. **130B**, 109 (1980); G. A. Ladinsky, Phys. Rev. D **39**, 2515 (1989).
[38] G. Valencia and A. Soni, Phys. Lett. B **263**, 517 (1991).
[39] S. Bar-Shalom, G. Eilam, and A. Soni, Phys. Rev. Lett. **80**, 4629 (1998).